IEEE Open Journal of
Nanotechnology

Received 19 October 2021; revised 23 November 2021; accepted 23 November 2021. Date of publication 30 November 2021; date of current version 14 December 2021. The review of this paper was arranged by Associate Editor Chang-Ki Baek.

Digital Object Identifier 10.1109/OJNANO.2021.3131165

Management of Phonon Transport in Lateral Direction for Gap-Controlled Si Nanopillar/SiGe Interlayer Composite Materials

DAISUKE OHORI [1,2,3], MIN-HUI CHUANG [2], ASAHI SATO [1], SOU TAKEUCHI [1], MASAYUKI MURATA [4], ATSUSHI YAMAMOTO [4], MING-YI LEE [2], KAZUHIKO ENDO [4], YIMING LI [2,3,5,6,7], JENN-HWAN TARNG [2,3,5,6], YAO-JEN LEE [8], AND SEIJI SAMUKAWA [1,3,4,6,9]

[1]Institute of Fluid Science, Tohoku University, Sendai 980–8577, Japan
[2]Department of Electrical and Computer Engineering, National Yang Ming Chiao Tung University, Hsinchu 30010, Taiwan
[3]Joint Research Center of National Yang Ming Chiao Tung University and Tohoku University, National Yang Ming Chiao Tung University, Hsinchu 30010, Taiwan
[4]National Institute of Advanced Industrial Science and Technology, Tsukuba 305–8568, Japan
[5]Institute of Communications Engineering, National Yang Ming Chiao Tung University, Hsinchu 30010, Taiwan
[6]Center for mm Wave Smart Radar System and Technologies, National Yang Ming Chiao Tung University, Hsinchu 30010, Taiwan
[7]Institute of Biomedical Engineering, National Yang Ming Chiao Tung University, Hsinchu 30010, Taiwan
[8]Taiwan Semiconductor Research Institute, Hsinchu 30010, Taiwan
[9]Advanced Institute for Materials Research, Tohoku University, Sendai 980–8577, Japan

CORRESPONDING AUTHORS: SEIJI SAMUKAWA; YIMING LI (e-mail: samukawa@ifs.tohoku.ac.jp; ymli@faculty.nctu.edu.tw).

This work was supported in part by Grant-in-Aid for Scientific Research(S) under Grant JP20H05649, in part by the Ministry of Science and Technology (MOST) Taiwan under Grants MOST 110-2221-E-A49-139, MOST 109-2221-E-009-033, and MOST 109-2634-F-009-030, and in part by the Center for mm Wave Smart Radar System and Technologies under the Featured Area Research Center Program within the framework for the Higher Education Sprout Project by the Ministry of Education in Taiwan.

ABSTRACT The phonon transport in the lateral direction for gap-controlled Si nanopillar (NP) /SiGe interlayer composite materials was investigated to eliminate heat generation in the channel area for advanced MOS transistors. The gap-controlled Si NP/SiGe composite layer showed 1/250 times lower thermal conductivity than Si bulk. Then, the phonon transport behavior in lateral direction could be predicted by the combination between the 3-omega measurement method for thermal conductivity and the Landauer approach for phonon transport in Si NP/$Si_{0.7}Ge_{0.3}$ interlayer composite structure. We found that the NP structure could regulate the phonon transport in the lateral direction by changing the NP gaps by preventing the phonon transportation from the drain region and the potential heat generation. As such, this structure achieves the first step toward phonon transport management in the same electron transportation direction of planar-type MOSFETs and represents a promising solution to heat generation for advanced CMOS devices.

INDEX TERMS Phonon transport control, Si nanopillar, neutral beam etching, simulation.

I. INTRODUCTION

IN recent years, the development of a smart society due to advances with Artificial Intelligence (AI) and Internet of Things (IoT) data communication has led to a greater demand for semiconductor devices [1]–[5]. The thermal budget involved in semiconductor operations such as device driving is increasing as the integration of semiconductor devices increases [6]. This has led to various problems related to performance reduction, device destruction, and limits to integration. In general, semiconductor devices need to have low heat generation and low power consumption. To improve the performance of the semiconductor device, a metal-oxide-semiconductor field-effect transistor (MOSFET) was designed with miniaturization, changing the structure from planer to Fin and nanosheet, and considering the material such as germanium [7]–[9]. In MOSFET, there are three causes of electron mobility reduction: Coulomb, roughness, and phonons. Electron scattering by phonons (electron-phonon scattering) is

particularly involved when the sub-10-nm advanced complementary-MOS (CMOS) reduces the carrier mobility. Heat is generated due to electrons passing through the channel region and at the interface of the channel and drain due to Joule heating. The excessive heat in the channel region of MOSFETs causes electron-phonon scattering and thus confines the maximum electron mobility.

The trends of electrical and thermal conductivity accumulation as a function of nanostructure size concerning mean free path (MFP) in Si have been reported [10]. The MFP of the electron is around less than 20 nm, whereas the MFP of the phonon accumulation needs to be more than a few hundred nm. In regions sized from 20 to a few hundred nm, phonons are sufficiently scattered, and electrons can thus be transferred without scattering. A nanostructure controlled within a region of this size can reduce the thermal conduction with keeping electron mobility. In our previous work, we achieved low thermal conductivity and high electrical conductivity by using a Si nanopillar (NP) with spin-on-glass or SiGe as a thermoelectric device [11], [12]. Moreover, a well-aligned and very tiny periodic structure was predicted that the structure of more than 5 periods localized the particular frequency phonon as a phononic crystal [13]. We, therefore, proposed using a MOSFET structure featuring a well-aligned Si NP/SiGe interlayer composite film as a channel region. Electrons can transfer the channel region to the lateral direction of the NP structure without any scattering, and then phonons are sufficiently scattered by the NP interface. Electron-phonon scattering occurs under the heat environment in the channel region based on the function of the temperature. The mainstream of the channel heating source was the transportation of Joule heat from the drain region to the channel region. Thus, well-phonon-scattered structures of well-ordered Si NP in the channel region work to prevent heat penetration from the drain and potential heat generation due to not disturbing the electron transportation. As a result, this structure enables the phonon-electron scattering to be eliminated, achieves higher electron mobility, and reduces the heat generation of the MOSFET. Therefore, a well-aligned Si NP structure with SiGe embedding will provide a high-performance MOSFET by increasing the electron mobility and controlling the phonon transport scattering.

In this study, to manage phonon transport in the channel region, we fabricated a well-aligned Si NP/$Si_{0.7}Ge_{0.3}$ with different NP gaps to investigate the phonon transportation in the lateral direction of thermal conductivity. We then performed measurements using the 3-omega method and simulation.

II. EXPERIMENT

Fig. 1 shows a schematic image of our neutral beam etching (NBE) system [14]. This system consists of an inductively coupled plasma (ICP) source and a carbon aperture plate, where the ultra-violet (UV) photon irradiation can be prevented, and energetic ions can be effectively converted into neutral beams by passing through the carbon aperture from plasma. The NBE can achieve ultra-precise nano-etching and perfectly suppress the formation of defects in the processed surface due to eliminating the incidence of charged particles and UV radiation onto the substrate.

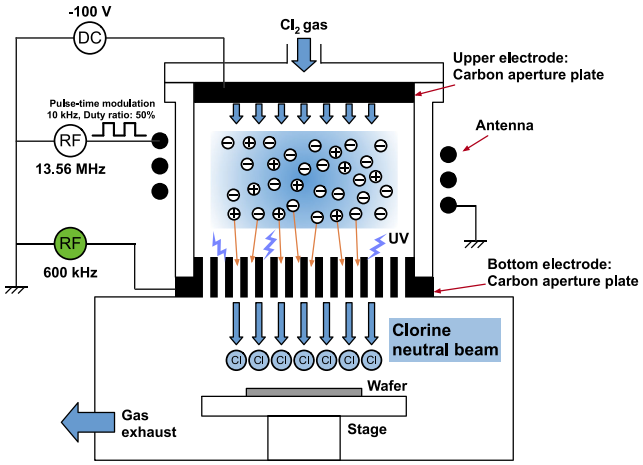

FIGURE 1. Neutral beam etching system.

The Si NP structure was fabricated on a silicon-on-insulator (SOI) wafer. The SOI wafer consists of a 100-nm-thick Si layer with a 140-nm-thick SiO_2 layer on a 725-nm-thick Si (100) substrate. First, the native SiO_2 film on the Si substrate was removed using a 1% HF solution for 2 min, and then, the controlled thin SiO_2 film (3.2-nm-thick) was synthesized by a neutral beam oxidation process [15]. Second, ferritin molecules were arranged with a spin-coating method [16]. The distance between ferritins was adjusted by a decorated-poly(ethylene-glycol) (PEG) with different molecular weights [17]. Specifically, the PEG molecular weights of 2k, 10k, and 20k (k = 1000) were 25, 40, and 60 nm of ferritin pitch (center-to-center distance of ferritin), respectively. Third, the coated ferritins were annealed to remove the surface protein shell at 400°C under oxygen atmosphere. After that, only iron cores remained on the surface of the thin SiO_2 film. The SiO_2 layer between the cores was then removed by H_2 radical treatment with NF_3 atmosphere and annealing. The NP structure was fabricated by chlorine NB etching for 25 min. After that, the remaining iron-oxide cores at the tip of the NP were removed with an HCl solution. Finally, the Si NP was embedded by $Si_{0.7}Ge_{0.3}$ with a low-pressure chemical vapor deposition (LPCVD) method.

The anisotropic thermal conductivity was performed using the 3-omega method, as shown in Fig. 2 [18]–[21]. Al line is for the heater, and the Al pad was connected to the voltage source and lock-in amplifier (Fig. 2(a)). With changing the Al heater width, heat distribution in the lateral direction was changed. Al line was prepared from 5 to 50 μm in width and 50 nm in thickness on deposited Al_2O_3 layer of 50 nm thickness. The stage temperature was at 300 K and the pressure of the sample room was 10^{-3} Pa. Obtaining value was waiting to be stable enough, after that, the value of acquired 50 times were averaged. Note here that the lateral direction of the thermal conductivity is more important for considering electron-phonon scatterings through the channel region

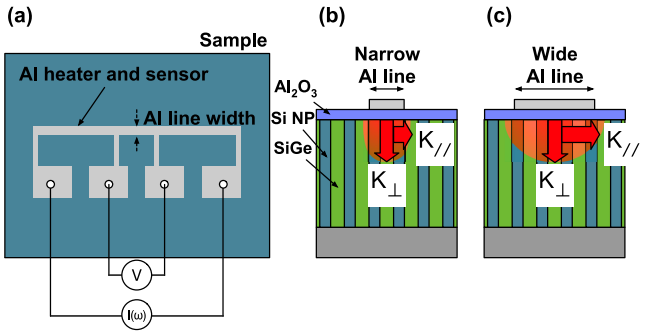

FIGURE 2. **Thermal conductivity measurement by 3-omega method. (a) Is a schematic image of the measurement sample with Al heater and sensor. The cross-sectional image of the (b) narrow and (c) wide Al line to measure thermal conductivity in a lateral direction.**

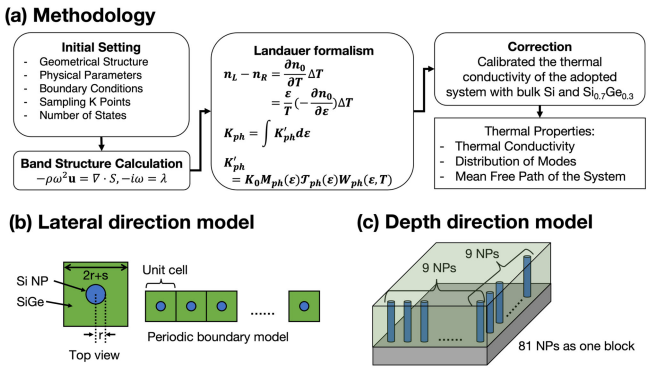

FIGURE 3. **(a) Calculation flow of anisotropic thermal conductivity and simulation model in (b) lateral direction and (c) vertical direction.**

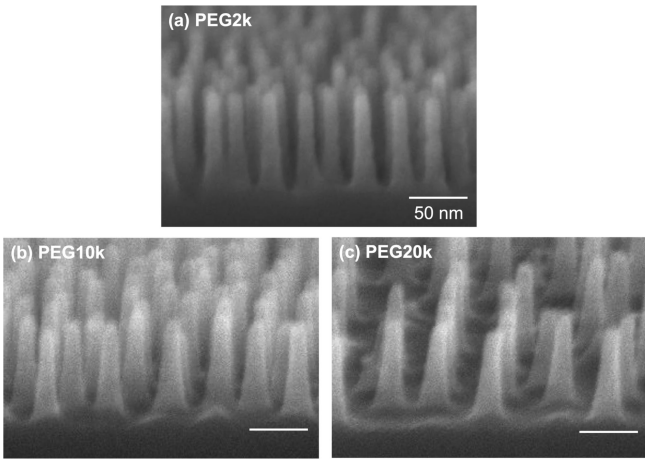

FIGURE 4. **Bird's-eye-view SEM images of Si NP structure using (a) PEG2k, (b) PEG10k, and (c) PEG20k ferritin molecules as an etching mask and NP center-to-center gap distribution. Si NP height was 90 nm.**

TABLE 1. **Diameter, Average (Pitch), Standard Deviation, and Density of Si NP Distribution**

Sample name (with PEG molecular weight)	Diameter (nm)	Average (nm)	Standard deviation (nm)	Density ($\times 10^{11}$ /cm^2)
12/13 (PEG2k)	12	25	5	1.8
13/27 (PEG10k)	13	40	8	0.68
13/47 (PEG20k)	13	60	12	0.34

in MOSFETs. Therefore, utilizing the 3-omega method to measure the thermal conductivity with a different line width of the Al heater is suitable to estimate the lateral or vertical direction of thermal conductivity [22], [23].

Thermal conductivity in bulk and lateral directions was simulated by the Landauer approach [24], as shown in Fig. 3. We modeled the Si NP structure with reference to the average actual Si NP height and pitch from SEM images. Other parameters (effective mass, bandgap, elastic constants, etc.) were as reported elsewhere [25]. For the lateral direction, we utilized a periodical boundary condition from the top-view NP model as shown in Fig. 3(b). The simulated model used an ideal structure in our Si NP alignment. In this study, the Si NP structure was fabricated to a large area of 30 mm square. For the simulation, the NP density is more than $10^{10} \sim 10^{11}$ /cm^2 if the simulation model was set along with the real structure. Thus, the lateral direction of the thermal conductivity was simulated by setting the periodic Si NP structure in the macroscopic scale. For the vertical direction, a 9 × 9 symmetric matrix was used as shown in Fig. 3(c).

III. RESULTS AND DISCUSSION

Fig. 4 shows bird's-eye-view SEM images of the Si NP structure using (a) PEG2k, (b) PEG10k, and (c) PEG20k ferritin molecules as an etching mask and NP center-to-center gap distribution. The height of the Si NP was 90 nm, and the diameters of (a), (b), and (c) were 12, 13, and 13 nm, respectively. As shown, the NP density from PEG2k to PEG20k decreased with the increase in PEG molecular weight. Table 1 shows the diameter, average, standard deviation, and density of the Si NP distribution. The NP gaps from edge-to-edge in Figs. 4(a)–(c) were 13, 27, and 47 nm, respectively. Hereafter, we refer to these samples as 12/13, 13/27, and 13/47 nm, with the numbers referring to the NP diameter/gap. NP distance was controlled within 20%. Fig. 5 shows cross-sectional SEM images of Si NP embedded by $Si_{0.7}Ge_{0.3}$. The thickness of the Si NP/$Si_{0.7}Ge_{0.3}$ composite film was 100 nm. $Si_{0.7}Ge_{0.3}$ was completely deposited into the Si NP structure.

Fig. 6 shows the thermal conductivity with error bars in the (a) vertical and (b) lateral directions for all Si NP/$Si_{0.7}Ge_{0.3}$ composite film samples measured by the 3-omega method [26], as well as the simulation results of the anisotropic thermal conductivity. For the vertical direction, the thermal conductivity increased slightly from 2.1 to 2.8 W/m/K when the gap was increased from 13 to 47 nm.

The thermal conductivity reduction was due to the interface scattering effect. As for the size effect, we found that the MPF of the phonon to vertical direction was the same as the composite film height at 100 nm. Under this condition,

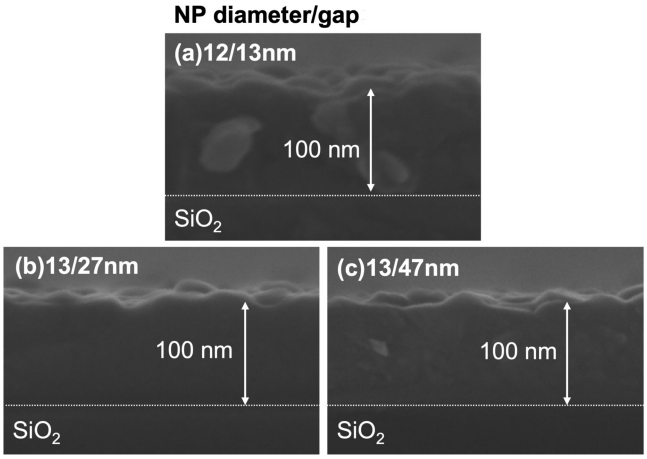

FIGURE 5. Cross-sectional SEM images of Si NP embedded by $Si_{0.7}Ge_{0.3}$ for (a) 12/13, (b) 13/27, and (c) 13/47 nm samples. The thickness of Si NP/$Si_{0.7}Ge_{0.3}$ composite film was 100 nm. $Si_{0.7}Ge_{0.3}$ was completely deposited into Si NP structure.

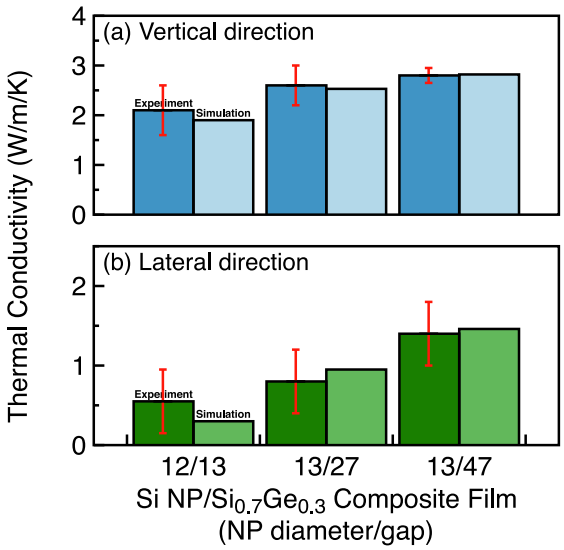

FIGURE 6. Thermal conductivity in (a) vertical and (b) lateral directions for all Si NP/$Si_{0.7}Ge_{0.3}$ composite film samples was measured using a 3-omega method. Simulation results of anisotropic thermal conductivity were drawn with each experimental result. Experimental results have error bar.

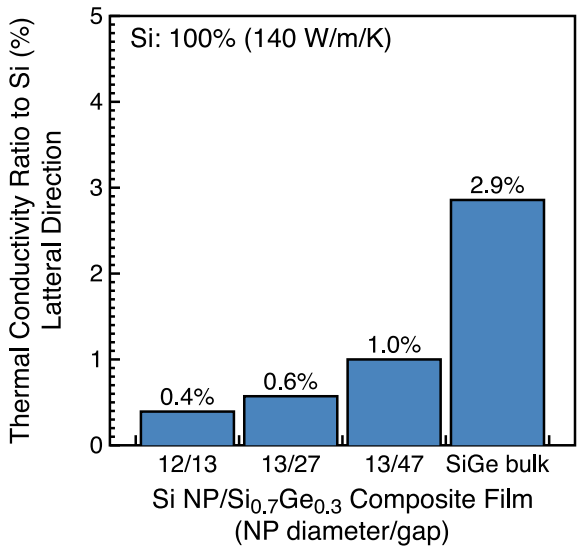

FIGURE 7. Thermal conductivity ratio to Si (100%, 140 W/m/K) of the lateral direction.

prior studies have indicated this it should decrease to 30% of ∼50 W/m/K of the thermal conductivity due to the volume ratio between Si and Ge [27], but our results showed that the thermal conductivity reduction was 10 times larger than that of the volume ratio. Moreover, all the NP samples demonstrated anisotropic thermal conductivity characteristics. The thermal conductivity in the lateral direction decreased to 25% less than that in the vertical direction. As stated earlier, the lateral phonon transport can be sufficiently scattered by the interface between NPs due to the longer MPF of the phonon accumulation. As a result, the thermal conductivity drastically decreases in the case of Si NP structures. Furthermore, the thermal conductivity can be controlled by increasing the NP gaps because the volume of the $Si_{0.7}Ge_{0.3}$ increases with a decreasing NP density. For the simulation results in Fig. 6, we estimated the thermal conductivity from the MFP of the bulk material and characteristics length for another internal scattering process [28], and as compared with the experimental results, the trends of all thermal conductivity results were in very good agreement. For the lateral direction of the 12/13 sample, the experimental result was 84% larger than the simulation results. This was because of the spread of the Si NP distribution. In this simulation, the NP alignment was a square grid with a periodical structure, whereas our NP arrangement includes a square grid, triangle grid, and random arrangement due to the self-assembly PEG-ferritin arrangement. Differences in the NP grid are known to lead to different heat fluxes [29]. As such, we should focus not only on ferritin density but also on ferritin distribution. The average and standard deviation of the distribution of the 12/13 sample was 25 nm, and 5 nm (Table 1), and the distribution was 18.5%. The distributions were 18.9, 20.0% for the 13/27, 13/47 samples, and all samples' errors were within 1.5%. As a result, in the narrow NP gap region, NP distribution affected thermal conductivity more strongly than in the wide region. We, therefore, conclude that a low thermal accumulation, i.e., a sparse density of states (DOS) in phonons, enables easy scattering due to the phonon accumulation of MPF.

Fig. 7 shows the thermal conductivity ratio to Si of the lateral direction. The thermal conductivity of the Si bulk and $Si_{0.7}Ge_{0.3}$ bulk were 140 and 4 W/m/K, respectively. The lateral phonon transport was appropriately scattered by the interface between NPs. As a result, the thermal conductivity drastically decreased. Furthermore, we found that the thermal conductivity could be controlled by increasing the NP gaps, as the volume of the $Si_{0.7}Ge_{0.3}$ increased with the decreasing NP density. The case of the 12/13, 13/27, and 13/47 sample was 0.4%, 0.6%, and 1.0%, respectively, that of Si bulk, although $Si_{0.7}Ge_{0.3}$ bulk was 2.9%. As a result, the phonon transport in the lateral direction was dramatically eliminated from 1/250 to 1/100 compared to Si bulk. A prior study [30] reported

that the mobility of a CMOS transistor operating in an extremely low temperature (4 K) became several tens of times higher than room temperature operation. This is presumably because the reduction of heat generation in the channel region eliminated the electron-phonon scatterings. We expect Si NP/$Si_{0.7}Ge_{0.3}$ composite structure to also significantly reduce electron-phonon scattering due to extremely low thermal conductivity, similar to Cryo-CMOS operation. Cryo-CMOS needs the cooling function to achieve the ignoring heat effect in the channel region. Si NP/$Si_{0.7}Ge_{0.3}$ composite structure provided the control and limitation of the phonon transportation from drain and generation in the channel region. It suggests that electrons can move in the channel region without any disturbance both structurally and energetically.

IV. CONCLUSION

We fabricated a well-aligned Si NP/$Si_{0.7}Ge_{0.3}$ interlayer composite film by changing the NP gaps from 13 to 47 nm. Phonon transport behavior through thermal conductivity was investigated by the 3-omega method and Lander approach for a thermally managed Si NP/$Si_{0.7}Ge_{0.3}$ interlayer composite structure. Results showed that our Si NP/$Si_{0.7}Ge_{0.3}$ interlayer composite film had a 1/100 times lower thermal conductivity than Si bulk thanks to controlling the phonon transports in the lateral direction. Moreover, a narrow NP gap led to effective phonon scattering due to the low thermal accumulation, i.e., the low density of the DOS of the phonon band. The results of thermal conductivity measurements and simulation clarified that the NP structure could regulate the phonon transport in the lateral direction by changing the NP gaps. Si NP/$Si_{0.7}Ge_{0.3}$ composite structure achieved the control and limitation of the phonon transportation from drain and generation in the channel region. As such, this structure achieves the first step toward the management of phonon transportation in the same electron transportation direction of the planar-type MOSFET and represents a promising solution to heat damage for advanced CMOS devices.

ACKNOWLEDGEMENT

Authors would like to thank Prof. J. Murota from the Micro System Integration Center in Tohoku University for helping to grow the SiGe film.

REFERENCES

[1] C. S. Aleman, N. Pissinou, S. Alemany, K. Boroojeni, J. Miller, and Z. Ding, "Context-aware data cleaning for mobile wireless sensor networks: A diversified trust approach," in *Proc. Workshop Comput., Netw. Commun.*, 2018, pp. 226–230.

[2] Y. Ai, M. Peng, and K. Zhang, "Edge computing technologies for internet of things: A primer," *Digit. Commun. Netw.*, vol. 4, pp. 77–86, 2018.

[3] A. Ghosh, D. Chakraborty, and A. Law, "Artificial intelligence in internet of things," *CAAI Trans. Intell. Technol.*, vol. 3, pp. 208–218, 2018.

[4] J. M. Tien, "Internet of things, real-time decision making, and artificial intelligence," *Ann. Data Sci.*, vol. 4, pp. 149–178, 2017.

[5] F. M. Simanjuntak, T. Ohno, S. Chandrasekaran, T.-Y. Tseng, and S. Samukawa, "Neutral oxygen irradiation enhanced forming-less ZnO-based transparent analog memristor devices for neuromorphic computing applications," *Nanotechnology*, vol. 31, 2020, Art. no. 26LT01.

[6] E. Pop, S. Sinha, and K. E. Goodson, "Heat generation and transport in nanometer-scale transistors," *Proc. IEEE*, vol. 94, pp. 1587–1601, 2006.

[7] W. Mizubayashi *et al.*, "Impacts of plasma-induced damage due to UV light irradiation during etching on Ge fin fabrication and device performance of Ge fin field-effect transistors," *Appl. Phys. Exp.*, vol. 10, no. 2, 2017, Art. no. 026501.

[8] Y. J. Lee *et al.*, "High performance complementary Ge peaking FinFETs by room temperature neutral beam oxidation for sub-7 nm technology node applications," in *Proc. IEEE Int. Electron Devices Meeting*, San Francisco, CA, USA, Dec. 2016, pp. 838–841.

[9] D. Ohori *et al.*, "High electron mobility germanium FinFET fabricated by atomic layer defect-free and roughness-free etching," *IEEE Open J. Nanotechnol.*, vol. 2, pp. 26–30, Jan. 2021.

[10] B. Qiu *et al.*, "First-principles simulation of electron mean-free-path spectra and thermoelectric properties in silicon," *Europhys. Lett.*, vol. 109, 2015, Art. no. 57006.

[11] A. Kikuchi, A. Yao, I. Mori, T. Ono, and S. Samukawa, "Extremely low thermal conductivity of high density and ordered 10 nm-diameter silicon nanowires array," *Appl. Phys. Lett.*, vol. 110, 2017, Art. no. 091908.

[12] A. Kikuchi, A. Yao, I. Mori, T. Ono, and S. Samukawa, "Composite films of highly ordered Si nanowires embedded in $SiGe_{0.3}$ for thermoelectric applications," *J. Appl. Phys.*, vol. 122, 2017, Art. no. 165302.

[13] Y. Guo *et al.*, "Thermal conductivity minimum of graded superlattices due to phonon localization," *APL Mater.*, vol. 9, 2021, Art. no. 091104.

[14] S. Samukawa, "Development of high-density plasma reactor for high-performance processing and future prospects," *Appl. Surf. Sci.*, vol. 192, pp. 216–243, 2002.

[15] M. Yonemoto *et al.*, "Low temperature, beam-orientation-dependent, lattice-plane-independent, and damage-free oxidation for three-dimensional structure by neutral beam oxidation," *Jpn. J. Appl. Phys.*, vol. 48, 2009, Art. no. 04C007.

[16] I. Yamashita, "Fabrication of a two-dimensional array of nano-particles using ferritin molecule," *Thin Solid Films*, vol. 393, pp. 12–18, 2001.

[17] R. Tsukamoto *et al.*, "Effect of PEGylation on controllably spaced adsorption of ferritin molecules," *Langmuir*, vol. 29, pp. 12737–12743, 2013.

[18] N. O. Birge, "Specific-heat spectroscopy of glycerol and propylene glycol near the glass transition," *Phys. Rev. B*, vol. 34, pp. 1631–1642, 1986.

[19] N. O. Birge and S. R. Nagel, "Wide-frequency specific heat spectrometer," *Rev. Sci. Instrum.*, vol. 58, pp. 1464–1470, 1987.

[20] D. G. Cahill, "Thermal conductivity measurement from 30 to 750 K: The 3ω method," *Rev. Sci. Instrum.*, vol. 61, pp. 802–808, 1990.

[21] T. Borca-Tasciuc, A. R. Kumar, and G. Chen, "Data reduction in 3ω method for thin-film thermal conductivity determination," *Rev. Sci. Instrum.*, vol. 72, pp. 2139–2147, 2001.

[22] A. Zhou, W. Wang, B. Yang, J. Li, and Q. Zhao, "Thermal conductivity study of micrometer-thick thermoelectric films by using three-omega methods," *Appl. Therm. Eng.*, vol. 98, pp. 683–689, 2016.

[23] D. Singhal *et al.*, "Measurement of anisotropic thermal conductivity of a dense forest of nanowires using the 3ω method," *Rev. Sci. Instrum.*, vol. 89, 2018, Art. no. 084902.

[24] J. Maassen and M. Lundstrom, "(Invited) The landauer approach to electron and phonon transport," *ECS Trans.*, vol. 69, pp. 23–36, 2015.

[25] M. Lee, Y. Li, M. Chuang, D. Ohori, and S. Samukawa, "Numerical simulation of thermal conductivity of SiNW–$SiGe_{0.3}$ composite for thermoelectric applications," *IEEE Trans. Electron Devices*, vol. 67, no. 5, pp. 2088–2092, May 2020.

[26] D. Ohori *et al.*, "Si Nanopillar/SiGe composite structure for thermally managed Nano-devices," in *Proc. 21st IEEE Int. Conf. Nanotechnol.*, Montreal, QC, Canada, 2021, pp. 199–202.

[27] T. Hori, T. Shiga, and J. Shiomi, "Phonon transport analysis of silicon germanium alloys using molecular dynamics simulations," *J. Appl. Phys.*, vol. 113, 2013, Art. no. 203514.

[28] A. J. H. McGaughey and A. Jain, "Nanostructure thermal conductivity prediction by Monte Carlo sampling of phonon free paths," *Appl. Phys. Lett.*, vol. 100, 2012, Art. no. 061911.

[29] R. Anufriev, A. Ramiere, J. Maire, and M. Nomura, "Heat guiding and focusing using ballistic phonon transport in phononic nanostructures," *Nat. Commun.*, vol. 8, 2017, Art. no. 15505.

[30] S. Hanamura, M. Aoki, T. Masuhara, O. Minato, Y. Sakai, and T. Hayashida, "Operation of bulk CMOS devices at very low temperatures," in *Proc. Symp. VLSI Technol. Dig. Tech. Papers*, 1983, pp. 46–47.